Effect of Substrate Surface Energy on Transcrystalline Growth and Its Effect on Interfacial Adhesion of Semicrystalline Polymers

Kilwon Cho,* Dohwan Kim, and Soong Yoon

Department of Chemical Engineering, Polymer Research Institute, Pohang University of Science and Technology, Pohang, 790-784, Korea

Received May 9, 2003; Revised Manuscript Received July 25, 2003

ABSTRACT: The effect of substrate surface energy on transcrystalline growth at the interface of a semicrystalline polymer and its effect on interfacial adhesion were investigated for substrates treated with various silane coupling agents. A thin film of isotactic polypropylene (iPP) crystallized on a high surface energy substrate (treated with γ-(aminopropyl)triethoxysilane) was composed entirely of transcrystallites. On the other hand, when the iPP film was crystallized on a low surface energy substrate (treated with perfluorodecyltrichlorosilane), the interface was dominated by spherulites, and only a very thin transcrystalline region (thickness $\sim$1 μm) was observed. The substrate surface energy was found to exert a significant influence on the crystallinity, density of nuclei, crystal microstructure (e.g., lamellar thickness and crystal orientation), and thickness of the transcrystalline region near the interface. The adhesion energy measured by the asymmetric double cantilever beam (ADCB) test increased strongly (from 1 to 100 J/m^2) with surface energy. Examination of the fractured specimens using atomic force microscopy and scanning electron microscopy revealed fibrillation of the iPP induced by the strong interfacial adhesion; this was found to be associated with the breakdown of the fibrils, which is the characteristic fracture mechanism of transcrystallites at the interface in high surface energy samples. At lower surface energies, however, cracking occurs at the boundary between the transcrystallites and the spherulites because of the weak boundary layer near the interface.

Introduction

Crystalline microstructural characteristics, such as crystallinity, crystal orientation, and density of nuclei, change on moving from a bulk to an interface. Transcrystallization caused by heterogeneous nucleation at the interface is a well-known phenomenon. The essential prerequisite for transcrystallization is the presence of a high density of active nuclei on the substrate surface. The closely packed nuclei hinder the lateral extension of spherulites, which are then forced to grow in one direction, namely perpendicular to the substrate.[1]

The possibility that surface nucleation behavior is determined by the surface energy of the substrate has also been considered. However, the exact mechanism of transcrystalline growth remains unclear. In general, extensive heterogeneous nucleation of polymer-melts at high-energy surfaces results in generation of transcrystals in the interfacial region.[2,3] Employing high-energy surfaces to facilitate the nucleation of a polymer melt is effective only if sufficient time is allowed for the polymer melt to achieve extensive and intimate contact with the substrate. Despite extensive work on such systems, most findings published to date have been qualitative in nature. Few attempts have been made to quantitatively characterize the ability of a given substrate to promote nucleation of a given polymer melt.[4−6]

According to polymer nucleation theory, the rate of heterogeneous nucleation[7,8] is given by

$$I = I_0 e^{-\Delta\varphi/kT} e^{-\Delta G^*/kT} \quad (1)$$

where I_0 is a constant nucleation rate, $\Delta\varphi$ is the activation energy for molecules to cross the phase boundary, ΔG^* is the critical excess free energy due to the creation of a nucleus, k is Boltzmann's constant, and T is the crystallization temperature. ΔG^* can be expressed as

$$\Delta G^* = \frac{16\sigma\sigma_e\Delta\sigma T_m^{0\,2}}{\Delta T^2 \Delta h_f^2} \quad (2)$$

where σ is the lateral surface energy, σ_e is the fold surface energy, $\Delta\sigma$ is the interfacial free energy difference, T_m^0 is the equilibrium melting temperature of the polymer, and Δh_f is the heat of fusion per unit volume of the polymer. The expression for ΔG^* in eq 2 differs markedly from that for homogeneous nucleation due to the introduction of $\Delta\sigma$, the interfacial free energy difference function. $\Delta\sigma$ is related to the creation of a new top surface, and it is best understood by breaking it down into its three basic components:[9]

$$\Delta\sigma = \gamma_{CS} + \gamma_{CM} - \gamma_{MS} \quad (3)$$

Here γ_{CS} is the crystal−substrate interfacial free energy, γ_{CM}[10] is the crystal−melt interfacial free energy ($\gamma_{CM} = \sigma$, defined as lateral surface free energy),[11−12] and γ_{MS} is the melt−substrate interfacial free energy. For hydrocarbons, for which dispersion forces dominate because there are no polar interactions, Fowkes[13] further expressed γ_{ab} as $(\gamma_a^{1/2} - \gamma_b^{1/2})^2$, where γ_a and γ_b represent the dispersion components of the surface tension for phases a and b. In particular, it seems reasonable to infer that the rate of heterogeneous nucleation is related to the interfacial free energy difference ($\Delta\sigma$). Therefore, in this paper, the interfacial free energy difference between the polymer and the substrate, $\Delta\sigma$, is selected as a major factor affecting transcrystalline growth.

* To whom all correspondence should be addressed. E-mail: kwcho@postech.ac.kr.

10.1021/ma034597p CCC: $25.00 © 2003 American Chemical Society
Published on Web 09/11/2003

Transcrystalline growth near the interface affects the interfacial adhesion as well as the mechanical properties of bulk.[14,15] Of particular interest is the proposal by several authors that a transcrystalline morphology improves the adhesion strength of an interface. Kwei et al.[16] and Matsuoka et al.[17] showed that the modulus of the transcrystalline region is higher than that of the bulk phase. Hsiao and Chen[18] used a microdebonding test to measure the interfacial strength of various Kelvar fiber-reinforced polymers. They found that the presence of a transcrystalline layer (TCL) increased the interfacial bond strength.[19,20] However, several studies have shown that the presence of transcrystals does not affect the interfacial strength,[21] or can even cause it to decrease.[22−34] Experiments on carbon fiber/PEEK composites have demonstrated that fiber composite systems in which a TCL is not induced have an interfacial shear strength[35] and transverse flexural strength[36] greater than those of the corresponding systems containing a TCL. In addition, Marom[14] attributed the effect of the TCL to the transcrystals having a preferred orientation relative to the fibers, thereby providing the surrounding matrix with a high rigidity and reduced thermal expansion in the fiber direction, which effectively lowered the residual thermal stresses. Meanwhile, transcrystallinity was found to have conflicting influences on the interfacial shear strength, depending on the matrix material. Thus, the effect of the presence of a TCL on interfacial strength is still under debate.

In the present study, we focused on the interface of isotactic polypropylene (iPP) and a silicon substrate treated with various silane coupling agents to change the surface energy. A flat silicon substrate was used to facilitate characterization of the crystalline microstructure. Interfacial adhesion strength was measured using an asymmetric double cantilever beam test instead of the conventional fiber pull-out test to exclude the frictional energy generated by the fiber pull-out test. The objectives of this work were (i) to investigate the effect of substrate surface energy on transcrystalline growth and (ii) to examine the effect of transcrystalline growth on interfacial adhesion of semicrystalline polymers. In addition, we investigated the correlations between the fracture mechanism and the crystalline microstructure near the interface with the surface energy.

Experimental Section

Materials. The polypropylene (PP) used in this study was a commercial molding grade Daelim Poly PP, supplied by Daelim Industrial Co. Its melt index was 12 g/10 min at 230 °C (ASTM: D1238). The PP granule was dried under vacuum at 50 °C for 24 h prior to use. The silicon wafer was cleaned with "Piranha" solution (70% vol H_2SO_4 + 30% vol H_2O_2) for 30 min at 100 °C and was washed with distilled water. The water contact angle was less than 5°. The silane coupling agents (Aldrich) used in this study were γ-(aminopropyl)-triethoxysilane (γ-APS), γ-chloropropyltriethoxysilane (γ-CPS), mercaptopropyltriethoxysilane (MPS), methyltriethoxysilane (MS), and perfluorodecyltrichlorosilane (FDS).

Surface Treatment and Characterization. For MS and MPS, anhydrous toluene solutions (50 mL) each containing one of the silane coupling agents (0.5 mL) were prepared under a nitrogen atmosphere.[37] The silicon wafers were placed in these solutions at 25 °C for 15 min. After silanization, the wafers were washed with toluene and baked for 30 min at 120 °C. Subsequently, the substrates were washed with toluene and methanol. Finally, the substrates were dried under vacuum. The same method was used for the other silane coupling agents, but the solvent was varied. In the cases of γ-APS and γ-CPS, distilled water was used instead of toluene in order to control the pH of the solution, while for FDS, *n*-hexane was used as the solvent. The sessile drop method was used to characterize the surface energy of the grafted silicon substrates and iPP films. From the contact angles with distilled water and diiodomethane, the characteristics of the surface energy were determined using the equation of Fowkes.[13]

Sample Preparation. The iPP films were prepared by compression molding for 10 min at 220 °C, followed by cooling to room temperature by running water under pressure. Each prepared iPP film (thickness ~200 μm) was melted between two treated silicon wafers at 220 °C for 10 min under nitrogen in a heating block to erase the thermal history. Then, the wafer−iPP system was rapidly transferred to another heating block, set at 120 °C. All the samples were crystallized at 120 °C under nitrogen for 24 h.

Microscopy. To study the crystalline morphology of the interface, an optical microscope was used in a polarized transmission mode (Axioplan, Zeiss). For this purpose, the film was detached from the substrate in water and a thin cross-section was produced using the ultramicrotome technique. The spherulitic morphology of the interface was observed by field emission scanning electron microscope (FE-SEM, Hitachi S-4200) with an accelerating voltage of 8 kV. The iPP film was etched in permanganic solution for 3 h and then dried under vacuum at room temperature for 2 days. A thin layer of thickness approximately 40 nm was sectioned from the stained sample using the ultramicrotome, and the sectioned specimens were further exposed to RuO_4 vapor for 1 h. Finally, they were examined under a JEOL-1200 transmission electron microscope (TEM) with an accelerating voltage of 120 kV.

X-ray Diffraction (Wide Angle and Grazing Incidence Angle). The crystalline orientation in the prepared films was qualitatively determined from $2\theta/\theta$ scans using a Rigaku RU200 X-ray diffractometer with Cu Kα radiation. X-ray measurements in the reflection mode were performed while the films were still lying flat on the silicon substrate. To investigate the crystalline microstructure of very thin films of the polymer by grazing incidence X-ray diffraction (GIXD), the iPP films were deposited by spin-coating on hot silicon wafer surfaces from solutions in pure tetrahydronaphthalene at 140 °C under argon to avoid oxidation of the polymer. Film thickness was controlled by adjusting the rotation speed and the concentration of the solution. The spin-coated samples were melted at 220 °C for 10 min and isothermally crystallized at 120 °C for 24 h. The diffraction patterns for the interface layer of the iPP films were obtained by GIXD. These experiments were conducted using a synchrotron X-ray radiation source (3C2 beamline, wavelength 1.598 Å) at the Pohang Accelerator Laboratory, Pohang, Korea.

Interfacial Adhesion Strength. Interfacial adhesion strength, G_i, was measured using the asymmetric double cantilever beam (ADCB) test applying the following equation:[38−41]

$$G_i = \left(\frac{3E_{iPP}E_{Si}h_{iPP}^{3}h_{Si}^{3}\Delta^2}{8a^4}\right)\left[\frac{C_{Si}^{2}E_{iPP}h_{iPP}^{3} + C_{iPP}^{2}E_{Si}h_{Si}^{3}}{(C_{Si}^{3}E_{iPP}h_{iPP}^{3} + C_{iPP}^{3}E_{Si}h_{Si}^{3})^2}\right]$$

$$C_{iPP} = \left(1 + 0.64\frac{h_{iPP}}{a}\right)$$

$$C_{Si} = \left(1 + 0.64\frac{h_{Si}}{a}\right) \quad (4)$$

where Δ is the thickness of the razor blade (0.1 mm), a is the crack length ahead of the blade, and E_i and h_i denote the Young's modulus and the thickness of material i, respectively. To satisfy the assumptions of the mechanical modeling of the ADCB test, the silicon/polymer interface cannot be tested directly and the specimen was modified by a glass plate.[40] As shown in Figure 1, we used the glass plate because it was required to stiffen the iPP film and to reduce the dissipative phenomena during the fracture test. To obtain a sufficient level

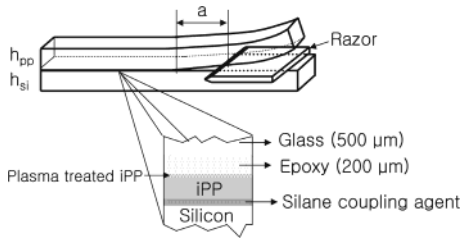

Figure 1. Schematic diagram of the iPP−silicon asymmetric double cantilever beam test sample showing details of the sandwich structure.

Table 1. Contact Angles, Surface Energy, and Thermodynamic Work of Adhesion of Silicon Substrates Modified with Various Silane Coupling Agents[a]

	contact angle (deg)		surface energy (mJ/m^2)				W_a
sample	water	diiodomethane	γ_s^p	γ_s^d	γ_s	$\Delta\sigma$	(mJ/m^2)
FDS	132	104	0.03	7.86	7.89	5.81	31.21
MS	70	56	12.91	24.06	36.97	1.41	59.26
MPS	57	50	20.02	25.18	45.21	1.18	62.98
γ-CPS	34	38	32.79	28.63	61.42	0.47	68.60
γ-APS	7	32	42.89	29.78	72.67	0.24	71.53

[a] γ_S^d: dispersion force component of surface energy. γ_S^p: polar force component of surface energy. $\gamma_S = \gamma_S^d + \gamma_S^p$. Thermodynamic work of adhesion, W_a : $W_a = 2(\gamma_S^d\gamma_{ipp}^d)^{0.5}+2(\gamma_S^p\gamma_{ipp}^p)^{0.5}$ (γ_{ipp}^d = 31.06 mJ/m^2, γ_{ipp}^p = 0.62 mJ/m^2).

of iPP/epoxy adhesion, the iPP surface was treated with oxygen plasma. The iPP/silicon joints were melted at 220 °C for 10 min and these were rapidly transferred to a heating block set at 120 °C, where these were left to crystallize for 24 h. A crack was initiated by inserting a razor blade into the iPP/silane-grafted silicon interface, as shown in Figure 1. It was allowed to propagate slowly for 24 h before measurement.

Fracture Surfaces. To study the failure mode and locus of failure, the fracture surfaces were examined by FE-SEM and atomic force microscopy (AFM) (Autoprobe CP, Park Scientific Instruments). AFM measurements were carried out in contact mode, using a silicon cantilever with a force constant of 0.24 N/m, and a scan rate of 0.5−1.0 Hz.

Results and Discussion

Dependence of Morphology on Substrate Surface Energy. Table 1 lists the calculated values of the surface energy (γ) and interfacial energy difference ($\Delta\sigma$) based on contact angle measurements for silicon substrates modified with various silane coupling agents. As expected, γ-APS, which contains an amine functional group, has the highest surface energy (72.67 mJ/m^2), and FDS, which contains a fluoroalkyl chain, has the lowest surface energy (7.89 mJ/m^2). As the surface energy increases from 7.89 to 72.67 mJ/m^2, the interfacial free energy difference decreases from 5.81 to 0.24 mJ/m^2. This difference in $\Delta\sigma$ is expected to lead to different crystalline morphologies in these systems.

Figure 2 shows polarized optical micrographs of the iPP thin films (200 μm) crystallized on silicon substrates with different surface energies, which were obtained by using γ-APS, γ-CPS, or FDS as the silane coupling agent. The iPP crystallized on the γ-APS-grafted silicon substrate, which has a high surface energy (72.67 mJ/m^2) and low interfacial free energy difference ($\Delta\sigma$ = 0.24 mJ/m^2), is composed entirely of a transcrystalline region. At this surface, heterogeneous nucleation is faster than homogeneous nucleation,[7,8] and hence there is no impingement of the bulk spherulites and only transcrystals grow. The iPP crystallized on the γ-CPS-grafted silicon substrate, which has a medium level of surface energy

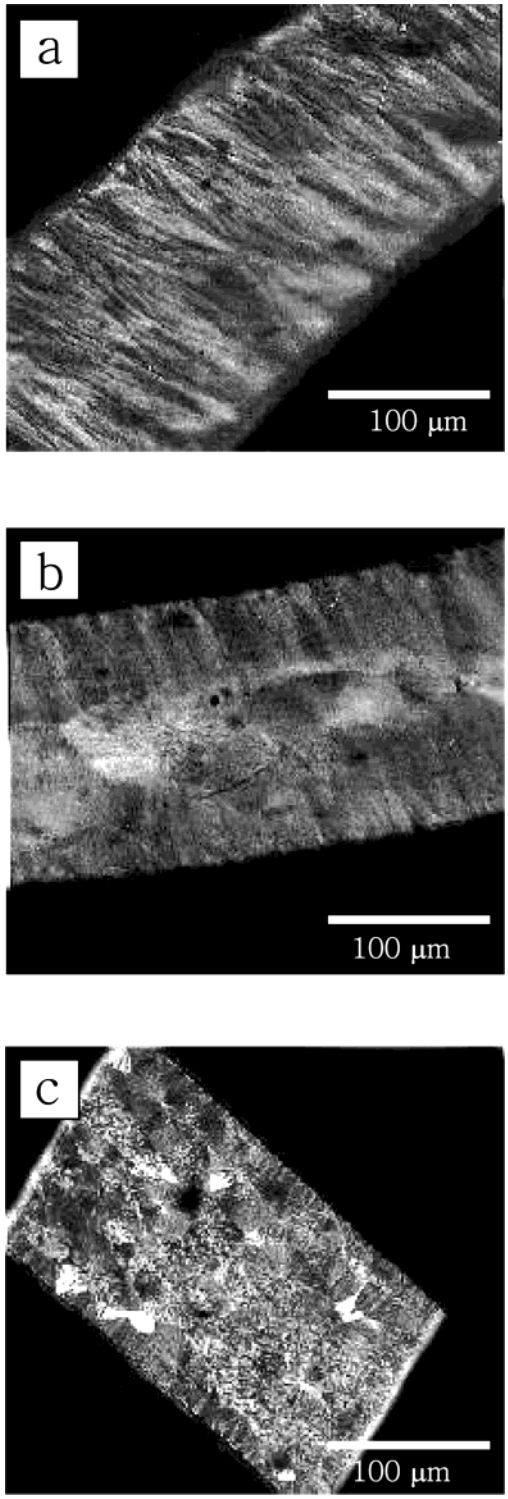

Figure 2. Polarized optical micrographs of the iPP thin film crystallized between two sheets of substrate modified with various silane coupling agents: (a) γ-APS (γ = 72.67 mJ/m^2); (b) γ-CPS (γ = 61.42 mJ/m^2); (c) FDS (γ = 7.89 mJ/m^2); Crystallization condition: 120 °C, 24 h.

(61.42 mJ/m^2; $\Delta\sigma$ = 0.47 mJ/m^2) consists of spherulites and a transcrystalline region. However, the presence of spherulites in the bulk is very rare. In addition, the shape of the spherulites observed in this system is nonspherical because growth toward the surfaces is hindered by impingement on transcrystals earlier than is the case for growth parallel to the surface. Yet another morphology is observed for the iPP crystallized in

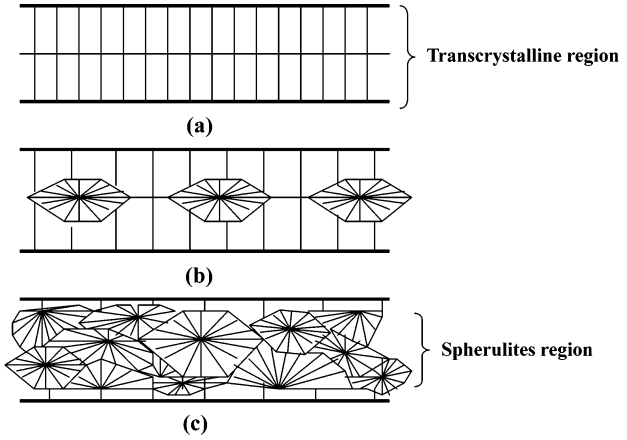

Figure 3. Schematic representation of crystalline morphologies of systems in Figure 1: (a) γ-APS treated; (b) γ-CPS treated; and (c) FDS treated.

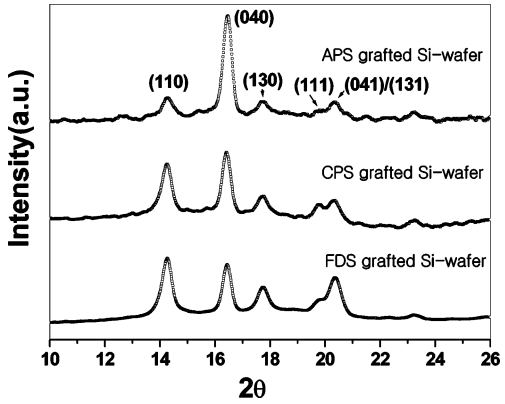

Figure 4. Influence of surface energy on the orientation of isotactic PP crystallized on a silicon substrate modified with a silane coupling agent: WAXD spectra.

contact with the FDS-grafted silicon substrate, which has a low surface energy (7.89 mJ/m^2; $\Delta\sigma = 5.81$ mJ/m^2). The most significant difference is that, in the bulk, a large number of spherulites start to grow before they impinge on the transcrystals. This suggests that the low-energy surface is not as effective for transcrystalline growth of iPP as the surfaces of higher energy. The morphologies at the low-, medium-, and high-energy surfaces are depicted schematically in Figure 3. The changes in morphology with varying surface energy are mainly related to the kinetics of crystallization; specifically, differences in the moments of nucleation of the crystals at the boundaries and in the bulk result in variations in the relative ranges of the TCL and bulk spherulites.[42] Apparently, the induction time for nucleation and crystallization is shorter at surfaces of higher energy. This can be clearly seen in Figure 2, which shows that the distance traveled by the transcrystalline front is larger than the distance traveled by the spherulite front prior to impingement. There is a competition between the bulk fraction and the transcrystalline fraction to occupy the volume of the material. In addition, because the range of the direct influence of the foreign surface on the crystallization process is limited, e.g, to a depth corresponding to one coiled macromolecule, the linear growth rates may become different for both fractions of crystals.

Crystalline Microstructure near the Interface. The influence of the substrate surface energy on the orientation of iPP crystals can be seen in the WAXD spectra shown in Figure 4. These spectra were recorded in reflection mode from a film of thickness approximately 200 μm. Thus, the diffraction pattern provides information on the bulk crystal structure. For the high-energy substrate surface (γ-APS-grafted surface), the diffraction intensity at the plane (040), which is a parallel plane to the substrate, shows a drastic increase compared to other planes such as the (110) and (130) planes. This increase in the diffraction intensity at the plane (040) compared to the (110) plane demonstrates that the lamellar crystals in the bulk are preferentially oriented perpendicular to the substrate, suggesting that the extent of the transcrystals increases with increasing substrate surface energy. These results are in accord with the structures observed in the polarized optical micrographs (Figure 2), which show that the spherulites disappear and transcrystals become dominant as the substrate surface energy increases. One can expect that the transcrystallization causes a higher degree of lamellar orientation at high energy substrate. In other words, the high surface energy of the γ-APS-grafted silicon substrate promotes the orientation of iPP crystals to a greater extent than the substrates of lower surface energy. In our experiment, it is clearly observed that the direction of the lamellar growth in the spherulites is random, whereas that in transcrystals is perpendicular to the substrate macroscopically in Figure 4.

To determine the crystallinity and crystalline microstructure near the polymer/substrate interface, we prepared iPP thin films of thickness 30 nm by spin-coating onto the γ-APS-, γ-CPS-, MPS-, or FDS-grafted silicon substrate. The crystalline microstructure in these thin films was characterized by grazing incidence angle X-ray diffraction (GIXD) measurements.[43,44] From the GIXD spectra, deconvolution of the diffractogram was carried out by a curve-fitting program to obtain quantitative information on the degree of crystallinity. The crystallinity increased from 53% to 62% on going from the substrate of lowest surface energy to that of highest energy. The low crystallinity at the surface with lowest surface energy (FDS-grafted silicon substrate) might be explained by the low degree of molecular perfection and the low mobility of isotactic PP chains, which limit the ability of chains to diffuse into the growing crystal front.

Comparison of the GIXD patterns of the thin films (Figure 5a) with the WAXD patterns of the bulk (Figure 4) reveals that the (111) and (041)/(13$\bar{1}$) peak intensities are lower for the thin interface layer than for the bulk. The decrease in the intensities of these peaks suggests that the *c* axis of the crystal in the interface layer was oriented more parallel to the substrate than in the bulk.[43] Figure 5b shows the ratio of the diffraction intensities at the (040) and (110) planes [$I_{(040)}/I_{(110)}$] as a function of substrate surface energy for the films of thickness 30 and 300 nm. This ratio increases with increasing substrate surface energy irrespective of film thickness, although the 300 nm thick film shows a more marked change in the intensity ratio. This result indicates that the degree of crystal orientation in a high-energy surface is different from that in a low-energy surface, which might be caused by the difference of the density of nuclei at the interface. That is, the closely packed nuclei hinder the lateral extension of lamellar crystals, which are then forced to grow in one direction, namely perpendicular to the substrate.

However, from a microscopic viewpoint, we can speculate that there are three regions on going from the

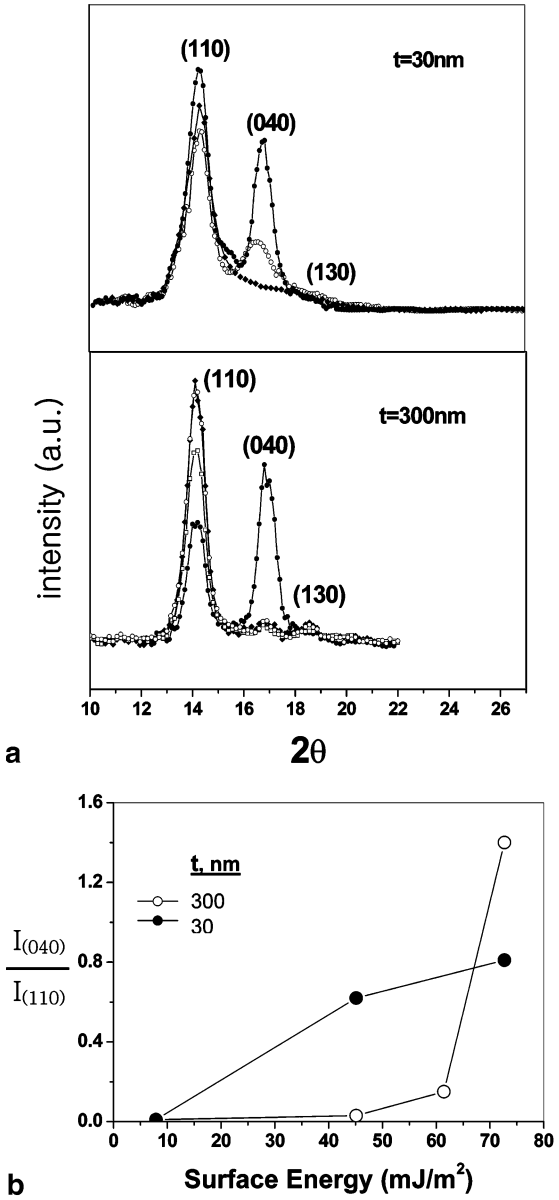

Figure 5. (a) Grazing incidence angle X-ray diffraction patterns of iPP thin films crystallized against silicon substrates modified with different silane coupling agents, incidence angle = 0.7°: (●) γ-APS, (□) γ-CPS, (○) MPS, (◆) FDS. (b). Ratio of the diffraction intensity for the (040) and (110) planes.

substrate to the bulk. The first region is that very close to the silane-coated substrate. In this region, there is some degree of lamellar orientation (as shown in Figure 5b) because the lateral extension of lamellar crystals is not hindered to a significant extent by neighboring lamellar crystals. Furthermore, as the surface energy increases, the crystals become preferentially oriented perpendicular to the substrate rather than parallel to the substrate. The second region is the intermediate region (30−300 nm from the substrate). In the case of a high-energy surface, the lateral extension of lamellar crystals in this region is hindered by neighboring lamellar crystals. Thus, the perpendicular orientation of lamellar crystals becomes dominant. For a low-energy surface, however, the parallel orientation of the lamellar crystals dominates because the density of nuclei is lower, and as a consequence there is not much hindrance by neighboring lamellar crystals. The change in

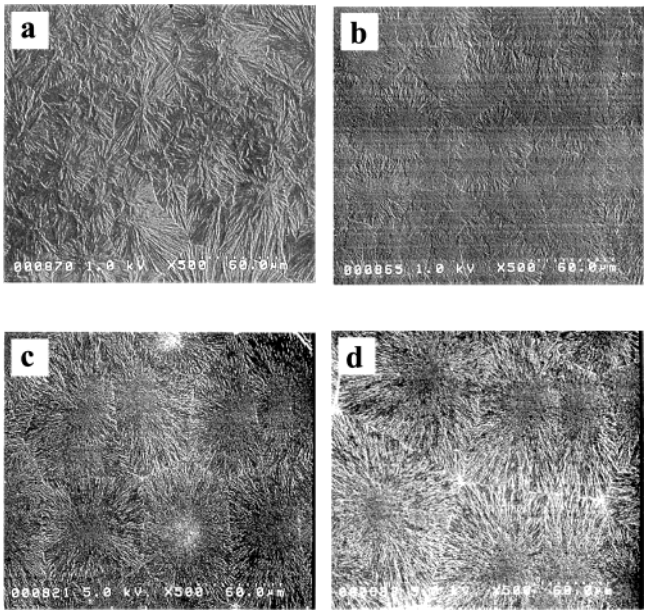

Figure 6. Scanning electron micrographs of the iPP surface for the iPP/substrate joints detached in distilled water: (a) γ-APS treated, spherulite size 25−30 μm; (b) γ-CPS treated (35−40 μm); (c) MS treated (60−70 μm); (d) FDS treated (100 μm).

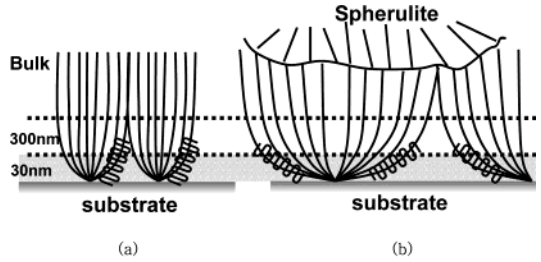

Figure 7. Schematic diagrams of the crystalline microstructure both near the interface and in the bulk for (a) a high surface-energy substrate and (b) a low-surface energy substrate.

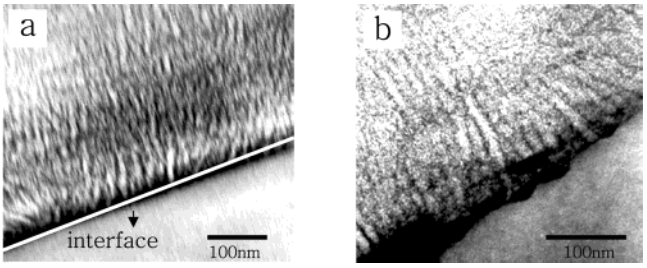

Figure 8. Transmission electron micrographs of the interface between iPP and (a) an FDS-grafted silicon substrate (surface energy 7.89 mJ/m^2), and (b) a γ-APS-grafted silicon substrate (surface energy 72.67 mJ/m^2).

the density of nuclei with increasing surface energy is confirmed by the size of the spherulites at the surface, as shown in Figure 6. From these results, we can construct schematic diagrams of the crystalline morphology near the interface at different substrate surface energies, as shown in Figure 7.

Crystalline Morphology near the Interface. Figure 8 shows high-resolution transmission electron micrographs of the interfacial region between the iPP and the silane-grafted silicon substrate for the systems with FDS-grafted and γ-APS-grafted silicon substrates (surface energies of 7.89 and 72.67 mJ/m^2, respectively).

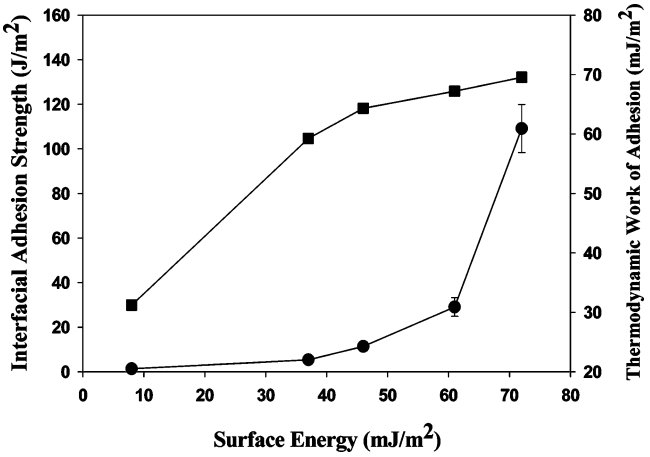

Figure 9. Adhesion strength and thermodynamic work of adhesion as a function of the surface energy of the silicon substrate modified with a silane coupling agent: (-●-) adhesion strength; (-■-) thermodynamic work of adhesion.

Both systems exhibit vertically oriented lamellar crystals near the interface. In fact, the transmission electron micrographs of these systems are very similar. To more clearly observe the spherulitic morphology near the substrate, the iPP films were detached in distilled water and the detached surfaces were examined by scanning electron microscopy. The resulting SEM micrographs, shown in Figure 6, clearly show the spherulites. In contrast to the TEM results, the spherulite size shows a marked dependence on substrate surface energy, increasing from 30 μm to 100 μm on decreasing the surface energy from 72.67 to 7.89 mJ/m^2. In contrast, the density of nuclei decreases with decreasing surface energy. The morphological changes with surface energy are related to the kinetics of the heterogeneous nucleation;[7,8] specifically, a low interfacial free energy difference ($\Delta\sigma$) promotes heterogeneous nucleation, causing the density of nuclei to increase, and as a consequence, the spherulite size decreases with increasing surface energy.

Interfacial Adhesion Strength. The adhesion strength of each interface was measured using the cleavage mode mechanical test known as the ADCB test. Use of the cleavage mode avoids the complications encountered in the conventional fiber pull-out test associated with the production of frictional energy. Figure 9 shows the adhesion strength of the interface vs the surface energy of the substrate. The adhesion strength is compared with the calculated values of the thermodynamic work of adhesion, W_a.[45] The adhesion strength of the iPP/silicon interface modified with γ-APS is about 100 times greater than that of the interface modified with FDS. The interfacial adhesion strength increases gradually with increasing surface energy up to a surface energy of 61.42 mJ/m^2, after which it suddenly jumps. The gradual enhancement of adhesion strength up to a surface energy of 61.42 mJ/m^2 is mainly due to the increase in the substrate surface energy since it controls both the crystalline microstructure and the thermodynamic work of adhesion near the interface. However, the marked increase in adhesion strength above a surface energy of 61.42 mJ/m^2 is caused by crystalline microstructure rather than thermodynamic work of adhesion.

To understand the relationship between the thermodynamic and mechanical aspects of the adhesion strength, we consider the relationship between the thermodynamic work of adhesion and the adhesion strength of the interface (Figure 10). As the thermodynamic work of adhesion increases from 31 to 68 mJ/m^2, the adhesion strength increases slightly. Above 68 mJ/m^2, however, the interfacial adhesion strength increases dramatically. These results suggest that the crystalline microstructure of the interface as well as the thermodynamic work of adhesion significantly affect the interfacial adhesion strength. The results shown in Figure 10 are consistent with the schematic picture of these systems presented in Figure 3; that is, spherulites in the bulk are the dominant feature at low surface energy (low W_a), whereas only transcrystallites are present at high surface energy (high W_a). One unexpected feature of Figure 10 is the sudden increase in the adhesion strength of the interface above $W_a = 68$ mJ/m^2. As will be seen in a later section, this increase can be attributed to the severe plastic deformation associated with cohesive failure rather than to adhesive failure.

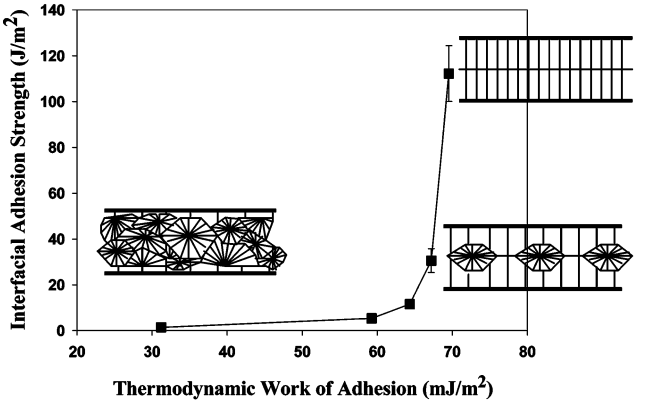

Figure 10. Relationship between thermodynamic work of adhesion and interfacial adhesion strength.

Table 2. Water Contact Angles on Silicon Substrates Modified with Various Silane Coupling Agents, before and after Fracture

samples	contact angle (deg) before fracture	contact angle (deg) after fracture
FDS	132.0 ± 3.4	110.2 ± 3.4
MS	70.2 ± 1.3	103.5 ± 1.8
MPS	57.2 ± 1.6	103.8 ± 2.4
γ-CPS	34.5 ± 1.4	106.4 ± 1.8
γ-APS	7.6 ± 0.5	112.0 ± 2.5
molded iPP	102 ± 2.3	

Analysis of Fracture Surfaces and Fracture Mechanism. To better understand the fracture mechanism and locus of failure, the fractured surfaces were examined through contact angle measurements, scanning electron microscopy (SEM) and atomic force microscopy (AFM). Water contact angles on silicon substrates modified with the various silane coupling agents (γ-APS, γ-CPS, MPS, MS, and FDS) after fracture were very close to those obtained for the pure isotactic PP matrix before jointing (Table 2). This result suggests that some residues of the isotactic PP remain anchored onto the silicon substrate. For the high-energy surface of the APS-treated substrate (Figure 11, parts a and b), the SEM images reveal fibrillation of the iPP induced by the strong interfacial adhesion, which is associated with the breakdown of the fibrils. The roughness of the fracture surface appears to be due to broken fibrils. Moreover, the thickness and roughness (ca. 200 nm) measured by AFM on the silicon substrate after fracturing are very different from those determined on the

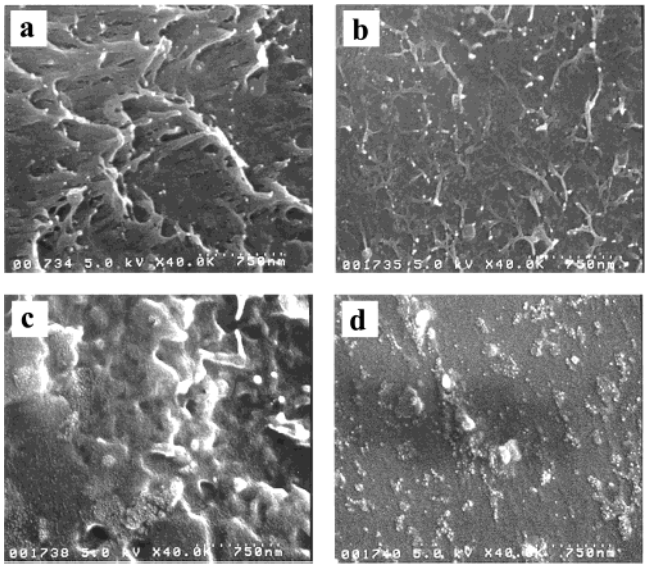

Figure 11. Scanning electron micrographs of the fracture surfaces of iPP/silicon substrates modified with two different silane coupling agents: γ-APS ((a) PP side, (b) wafer side); FDS ((c) PP side, (d) wafer side).

silicon substrate before jointing (Figure 12). The height profile shows a damaged fracture pattern, which suggests indirectly but clearly that the layer thickness results from the cohesive failure of the matrix. These results lead us to conclude that, for the high-energy surface, large-scale plastic deformation occurred on the iPP side and cracking proceeded by the breakdown of PP fibrils, as depicted schematically in Figure 12.

In the case of the silicon substrate modified with FDS (low-energy surface), the failure is almost entirely interfacial, although not completely so, as indicated by the observation of iPP residues on the separated silicon substrate in the SEM micrographs of the fractured silicon substrate (Figure 11, parts c and d). On the basis of this observation, it can be speculated that by decreasing the surface energy, the inter-crystalline microcrack might occur at the boundary between the transcrystallites and the spherulites in the bulk because of the weak boundary layer near the interface. Of course, the thermodynamic work of adhesion is less for a low-energy surface than for a high-energy surface. Therefore, the crack could propagate across the transcrystal−substrate interface even though the crack was initiated at the boundary between the transcrystallites and the spherulites in the bulk. For this system, AFM measurements (Figure 13) reveal that the roughness of the silicon substrate after fracturing is not the same as before jointing. However, fracturing phenomena on the silicon substrate appear inhomogeneously unlike those of the high surface energy system. These results imply the existence of diverse fracture mechanisms, as mentioned above. The AFM results, shown in Figure 13, support the existence of both mechanisms for crack propagation, namely (1) crack propagation across the interface of the iPP/silicon substrate modified with silane and (2) crack propagation across the boundary of the transcrystallites and the spherulites in the bulk because the boundary is very weak.

Figure 13 shows a schematic representation of the two modes of crack propagation in the FDS-treated substrate: near the interface and in the bulk. Once the crack is initiated toward the bulk, it prefers to propagate along the so-called intercrystalline weak path. In coarse spherulitic materials (Figure 13), plastic deformation can occur in the boundary zones, whereas the transcrys-

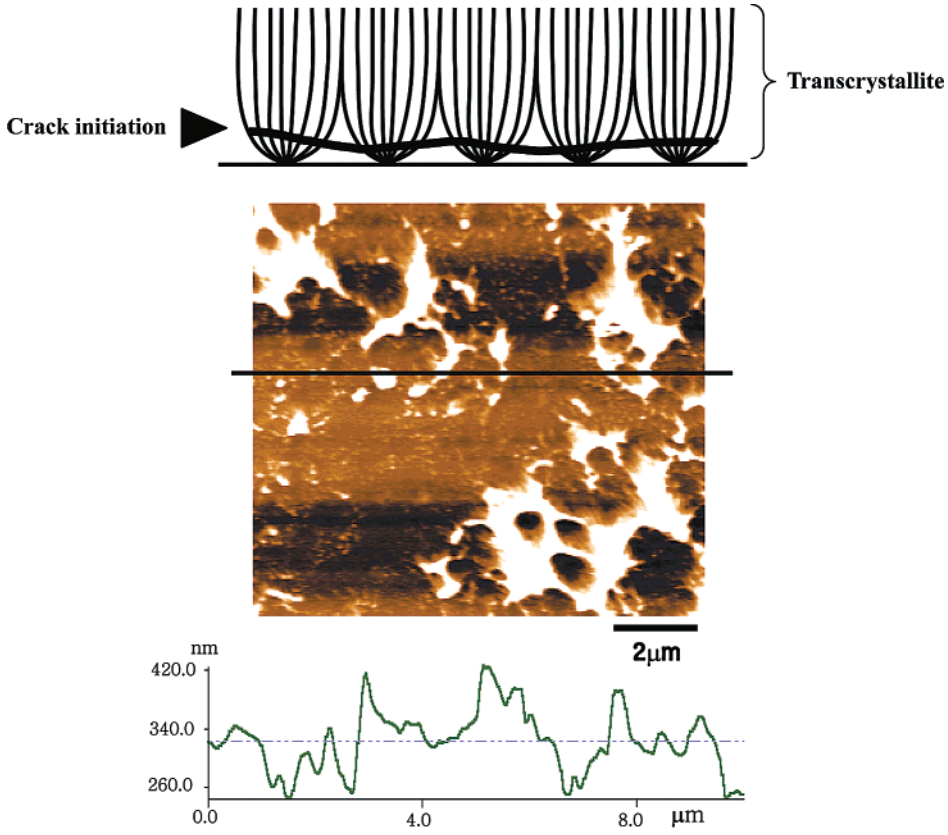

Figure 12. Topography and height profile of the γ-APS-modified silicon substrate after fracturing.

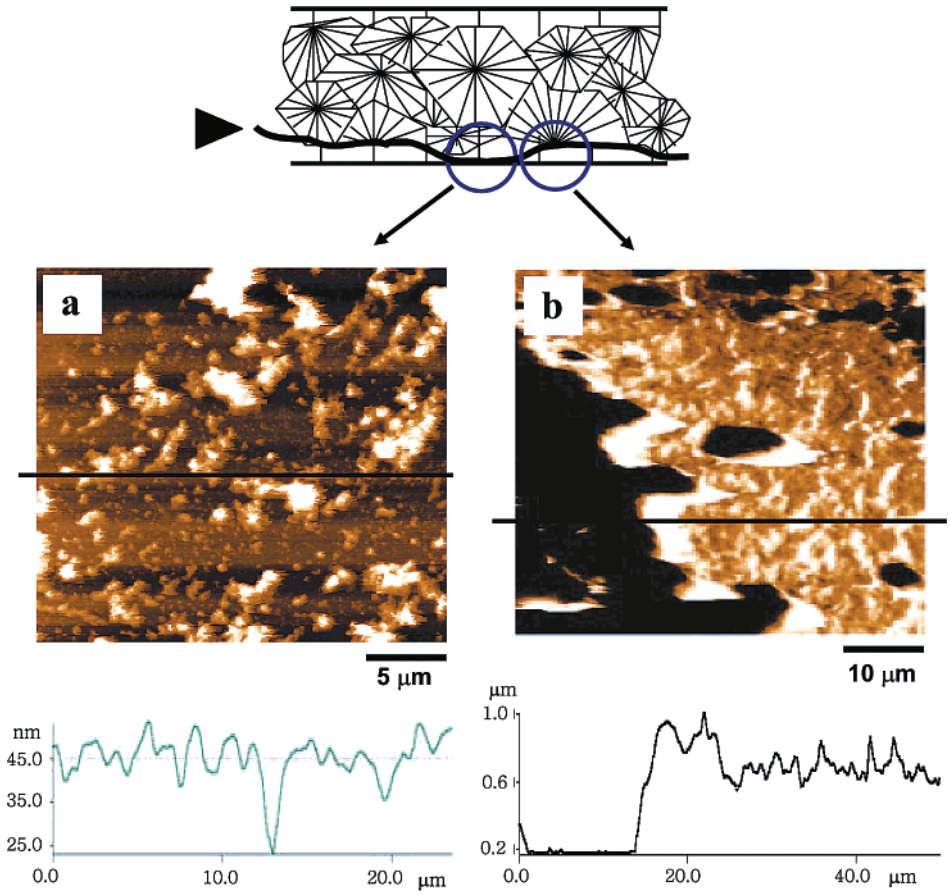

Figure 13. Topography and height profile of the FDS-modified silicon substrate after fracturing: (a) crack propagation across the interface, and (b) crack propagation across the intercrystalline boundary between the transcrystals and spherulites.

tals themselves may remain almost undeformed because of their relatively stiff characteristics. The stiffness enhancement with TCL is caused by the higher crystallinity and perpendicular lamellar morphology of transcrystals, which generates higher normal compression stress on the silicon substrate. The crack can propagate along the intercrystalline boundary because this boundary might be crossed only by short end-sections of lamellae and by some inter-crystalline links. Of course, crack propagation is also observed at the substrate-transcrystal interface, which has a low thermodynamic work of adhesion (31 mJ/m^2).

Comparison of Cleavage Test with Pull-Out Test. The pull-out test has been widely used to measure the interfacial shear strength in fiber-reinforced composite materials. However, the utility of this test for determining interfacial adhesion strength is limited by the fact that it produces frictional energy at the interface between the fiber and the polymer matrix. In general, the interfacial shear strength, τ_i, can be calculated from the following equation:

$$\tau_i = \frac{F_{max}}{\pi DL} \tag{5}$$

where F_{max} is the maximum tensile load, and D and L are the fiber diameter and the embedded fiber length, respectively.[46] If the thickness of the transcrystal increases with the surface energy and the interface between spherulites and transcrystals is weak, failure occurs at the interface and the apparent diameter of the pulled-out fiber, D, increases with increasing thickness of the transcrystal. Therefore, the frictional force as well as the maximum tensile load increases if the thermodynamic work of adhesion is sufficiently high, even though the transcrystal-spherulite interface is not strong. Under such circumstances, it is not possible to compare the critical adhesion strength caused by the different morphological features. In addition, the maximum tensile load increases continuously with transcrystal thickness. Thus, in our experiments, to compare the morphological effect on the adhesion strength as well as to determine the exact fracture mechanism, we used a cleavage mode test known as the asymmetric double cantilever beam test as the fracture test. By using this method, the frictional force contribution could be excluded and only the morphological effect caused by the substrate could be obtained. It should be noted that by using this method, we can clearly evaluate the morphological effect on the interfacial adhesion strength as well as its effect on the fracture mechanism.

Conclusions

The adhesion between iPP and a silane-grafted silicon substrate was shown to be enhanced by increasing the surface energy of the substrate, which significantly affects the transcrystalline growth. A thin iPP film crystallized on a silicon substrate of high surface energy was found to consist of only transcrystallites. In the thin iPP film on a low surface energy substrate, however, spherulites are the dominant feature and the interface contains only a very thin transcrystalline region. The surface energy was also found to affect microstructural characteristics such as density of nuclei, crystal orientation, and crystallinity.

The adhesion strength of the interface was found to increase significantly with increasing surface energy of the substrate, as determined using the asymmetric double cantilever beam test. The enhancement of interfacial adhesion strength for substrates of higher surface energy is attributed to the increase in transcrystalline growth near the interface as well as the thermodynamic work of adhesion with increasing substrate surface energy.

In the high surface energy sample, fibrillation of the iPP induced by the strong interfacial adhesion and subsequent breakage of the fibrils was found to be the characteristic fracture mechanism of transcrystallites at the interface. At lower surface energies, on the other hand, a microcrack was found to occur at the boundary between the spherulites and the transcrystallites due to the weak boundary layer near the interface.

Acknowledgment. The authors would like to thank the National Research Laboratory Project (Ministry of Science and Technology of Korea), Korea Science and Engineering Foundation (Contract No. R01-2000-000-00335-0) and the Ministry of Education of Korea for its support through its BK21 Program and the Pohang Acceleratory Laboratory for providing the synchrotron radiation source at the 3C2 beamline used in this study.

References and Notes

(1) Fitchmun, D. R.; Newman, S. *J. Polym. Sci., Part A2* **1970**, *8*, 1545.
(2) Schonhorn, H. *Macromolecules* **1991**, *24*, 3569.
(3) Billon, N.; Henaff, V.; Pelous, E.; Haudin, J. M. *J. Appl. Polym. Sci.* **2002**, *86*, 725.
(4) Wang, C.; Liu, C. R. *Polymer* **1999**, *40*, 289.
(5) Assouline, E.; Pohl, S.; Fulchiron, R.; Lustiger, A.; Wagner, H. D.; Marom, G. *Polymer* **2000**, *41*, 7843.
(6) Pattanayek, S. K.; Kim, D. H.; Cho, K. W. *Macromolecules* **2003**, submitted for publication.
(7) Wunderlich, B. *Macromolecular Physics*; Academic Press: New York, 1976; Vol. 2, Chapter 5.
(8) Binsbergen *J. Polym. Sci. Polym. Phys. Ed.*, **1973**, *11*, 117.
(9) Cherry, B. W. *Polymer Surfaces*; Cambridge University Press: London, 1981.
(10) $\gamma_C = 31.06$ mJ/m^2 was obtained by contact angle measurement, and $\gamma_M = 20.5$ mJ/m^2 was obtained by the Guggenheim equation, $\gamma = \gamma_0(1 - T/T_c)^{11/9}$; $\gamma_{CM} = (\gamma_C^{1/2} - \gamma_M^{1/2})^2$: Guggenheim, E. A. *J. Chem. Phys.* **1945**, *13*, 253.
(11) Karger-Kocis, J. *Nucleation in Polypropylene*; Chapman & Hall: London, 1995; Vol. 1.
(12) Ishida, H.; Bussi, P. *Macromolecules* **1991**, *24*, 3569.
(13) Fowkes, F. M. *Ind. Eng. Chem.* **1964**, *56*, 40.
(14) Klein, N.; Marom, G.; Pegoretti, A.; Migliaresi, C. *Composites* **1995**, *26*, 707.
(15) Amitay-Sadovsky, E.; Cohen, S. R.; Wagner, H. D. *Mcromolecules* **2001**, *34*, 1252.
(16) Kwei, T. K.; Schonhorn, H.; Frisch, H. L. *J. Appl. Phys.* **1967**, *38*, 2512.
(17) Matsuoka, S.; Daane, J. H.; Bair, H. E.; Kwei, T. K. *J. Polym. Sci., Polym. Lett. Ed.* **1968**, *6*, 87.
(18) Chen, E. J. H.; Hsiao, B. S. *Polym. Eng. Sci.* **1992**, *32*, 66.
(19) Hsiao, B. S.; Chen, E. J. *Controlled Interphases in Composite Materials*; Ishi-da, H., Ed.; Elsevier Sci.: New York, 1990; p 613.
(20) Chang-Mou, W.; Ming, C.; Karger-Kocsis *J. Polymer* **2001**, *42*, 199.
(21) Gati, A.; Wagner, H. D. *Macromolecules* **1997**, *30*, 3933.
(22) Tordella, J. P. *J. Appl. Polym. Sci.* **1970**, *14*, 1627.
(23) Nakao, K. *J. Adhes.* **1972**, *4*, 95.
(24) Xavier, S. F.; Sharma, Y. N. *Makromol. Chem.* **1984**, *127*, 145.
(25) Bassell, T.; Hull, D.; Shortall, J. B. *Faraday Spec. Discuss. Chem. Soc.* **1972**, *2*, 137.
(26) Nagae, S.; Otsuka, Y.; Nishida, M.; Shimizu, T.; Takeda, T.; Yumitori, S. *J. Mater. Sci. Lett.* **1995**, *14*, 1234.
(27) Felix, J. M.; Gatenholm, P. *J. Mater. Sci.* **1994**, *29*, 3043.
(28) Yue, C. Y.; Cheung, W. L. *J. Mater. Sci.* **1992**, *27*, 3181.
(29) Huson, M. G.; Mcgill, W. J. *J. Polym. Sci., Part B: Polym. Phys.* **1985**, *23*, 121.
(30) Lustiger, A. *Polym. Compos.* **1992**, *13*, 408.
(31) Folkes, M. J.; Wong, W. K. *Polymer* **1987**, *28*, 1309.
(32) Hoecker, F.; Karger-Kocsis *J. Polym. Bull. (Berlin)***1993**, *31*, 707.
(33) Moon, C. K. *J. Appl. Polym. Sci.* **1994**, *54*, 73.
(34) Wang, C.; Hwang, L. N. *J. Polym. Sci., Part B, Polym. Phys.* **1996**, *34*, 1435.
(35) Gaur, U.; Desio, G.; Miller, B. *APE. ANTEC. Technol. Pap.* **1989**, *135*, 1513.
(36) Peacock, J. A.; Fife, B.; Nield, E.; Crick, R. A. In *CompositeInterfaces*; Ishida, H., Koenig, J. L., Eds.; North-Holland: New York, 1986.
(37) Moon, J. H.; Shin, J. W.; Kim, S. Y.; Park, J. W. *Langmuir* **1996**, *12*, 4621.
(38) Kanninen, M. F. *Int. J. Fract.* **1973**, *9*, 83.
(39) Boucher, E.; Folkers, J. P.; Hervet, H.; Le'ger, L.; Creton, C. *Macromolecules* **1996**, *29*, 774.
(40) Smith, J. M.; Kramer, E. J.; Xiao, F.; Hui, C. Y.; Reichert, W.; Brown, H. R. *J. Mater. Sci.* **1993**, *28*, 4234.
(41) Cho, K.; Li, F. *Macromolecules* **1998**, *31*, 7495.
(42) Piorkowska, E. *Colloid Polym. Sci.* **1997**, *275*, 1046.
(43) Laurens, C.; Ober, R.; Creton, C.; Leger, L. *Macromolecules* **2001**, *34*, 2932.
(44) Kawamoto, N.; Mori, M.; Nitta, K.; Yui, N.; Terano, M. *Macromol. Chem. Phys.* **1998**, *199*, 261.
(45) Calculated by the equation in Table 1.
(46) Gati, A.; Wagner, H. D. *Macromolecules* **1997**, *30*, 3933.

MA034597P